ACS Biomaterials SCIENCE & ENGINEERING
Cite This: ACS Biomater. Sci. Eng. 2019, 5, 603−612
Article
pubs.acs.org/journal/abseba

# Designing Bacterial Chemotactic Receptors Guided by Photonic Femtoliter Well Arrays for Quantifiable, Label-Free Measurement of Bacterial Chemotaxis

Tzila Davidov,[*,†,‡] Naor Granik,[†,§] Sharbel Zahran,[†,‡] Heidi Leonard,[†,‡] Inbal Adir,[⊥] Ofek Elul,[‡] Tal Fried,[∥] Asif Gil,[‡] Bar Mayo,[#] Shilo Ohayon,[‡] Shiran Sarig,[‡] Nofar Shasha,[∥] Shirane Tsedef,[‡] Shani Weiner,[‡] Michal Brunwasser-Meirom,[‡] Alexandra Ereskovsky,[‡] Noa Katz,[‡] Beate Kaufmann,[‡] Yuri Haimov,[‡] Ester Segal,[‡,△] and Roee Amit[*,‡,△]

[‡]Department of Biotechnology and Food Engineering, [§]Department of Electrical Engineering, [⊥]Department of Computer Science, [∥]Department of Chemical Engineering, [#]Department of Mechanical Engineering, and [△]The Russell Berrie Nanotechnology Institute, Technion−Israel Institute of Technology, Haifa 3200003, Israel

Supporting Information

**ABSTRACT:** Whole cell bioreporters, such as bacterial cells, can be used for environmental and clinical sensing of specific analytes. However, the current methods implemented to observe such bioreporters in the form of chemotactic responses heavily rely on microscope analysis, fluorescent labels, and hard-to-scale microfluidic devices. Herein, we demonstrate that chemotaxis can be detected within minutes using intrinsic optical measurements of silicon femtoliter well arrays (FMAs). This is done via phase-shift reflectometric interference spectroscopic measurements (PRISM) of the wells, which act as silicon diffraction gratings, enabling label-free, real-time quantification of the number of trapped bacteria cells in the optical readout. By generating unsteady chemical gradients over the wells, we first demonstrate that chemotaxis toward attractants and away from repellents can be easily differentiated based on the signal response of PRISM. The lowest concentration of chemorepellent to elicit an observed bacterial response was 50 mM, whereas the lowest concentration of chemoattractant to elicit a response was 10 mM. Second, we employed PRISM, in combination with a computational approach, to rapidly scan for and identify a novel synthetic histamine chemoreceptor strain. Consequently, we show that by using a combined computational design approach, together with a quantitative, real-time, and label-free detection method, it is possible to manufacture and characterize novel synthetic chemoreceptors in *Escherichia coli* (*E. coli*).

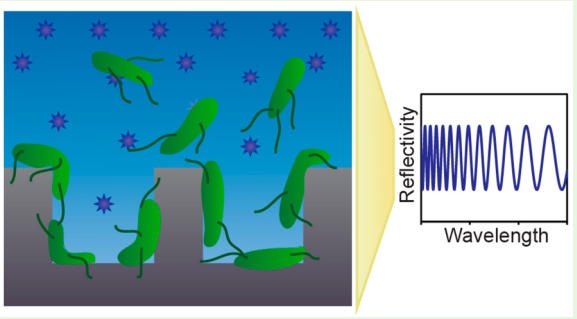


**KEYWORDS:** *chemotaxis, diffraction, microstructures, optical biosensor, synthetic biology*

## INTRODUCTION

Bacterial chemotaxis is the biasing of bacterial movement in response to an external chemical stimulus. This system enables bacteria to sense the chemical composition of their immediate environment and quickly adapt to changes, moving away from repellents or toward attractants, thus ensuring their survival. Furthermore, it is characterized by specific responses, high sensitivity, and a dynamic range,[1,2] making it useful in whole-cell living bacterial bioreporting to detect specific chemicals in environmental[3] or clinical samples.[4,5] Although conventional bioreporters for chemical detection rely on lengthy gene expression or protein production,[6] chemotactic bacterial cells have the ability to detect chemical gradients in milliseconds.[7]

Several groups have developed methods for observing chemotaxis in bacterial populations, most of which incorporate microfluidic chambers for lab-on-a-chip applications, notably a T-shaped microfluidic device under flow[8] and a Y-shaped design for static conditions.[9] Various, more complex, gradient generating chambers have also been employed,[10] including a Christmas tree design gradient generator[11] and a three-channel linear gradient generator for quantitative chemotaxis.[12] Additionally, parallel channels linked by pores have been used to qualitatively and quantitatively analyze bacterial chemotaxis.[13,14]

Although bacteria have naturally evolved to detect a variety of beneficial or harmful analytes, their endogenous chemoreceptors are often ill-suited for many desired applications. As a result, a substantial effort in synthetic biology has been directed toward expansion of the bacterial analyte detection repertoire via design and development of novel genetically

Received: November 16, 2018
Accepted: January 2, 2019
Published: January 2, 2019






DOI: 10.1021/acsbiomaterials.8b01429
ACS Biomater. Sci. Eng. 2019, 5, 603−612

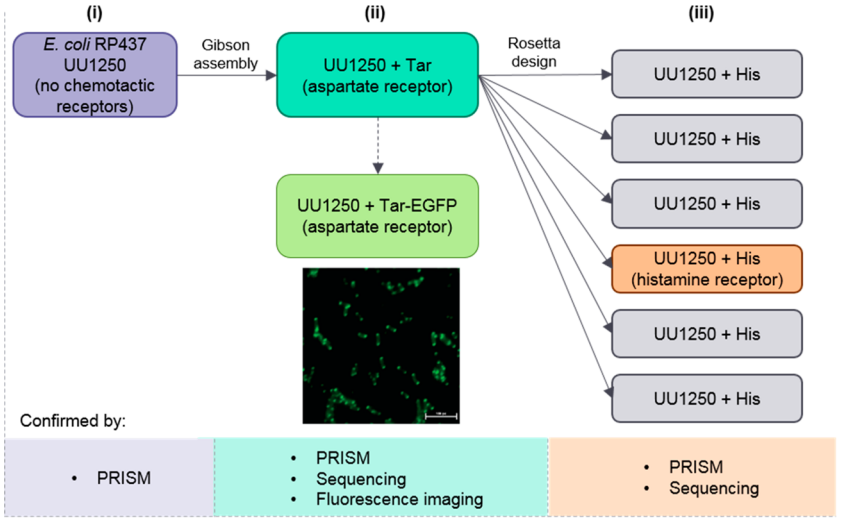


**Figure 1.** Flowchart representing the synthesis of the chemotactic *E. coli* variants. (i) *E. coli* RP437 UU1250, a chemotactically deficient strain, was used as a parental strain for (ii) UU1250-Tar, which was constructed using a Gibson Assembly cloning reaction. Incorporation of the pTSB1C3-*tar* plasmid was confirmed by PRISM chemotaxis assays and genomic sequencing. Incorporation of the similar pTSB1C3-*tar*-EGFP plasmid was confirmed by fluorescence microscopy, in which EGFP, and thus Tar, was expressed at the localized poles of the cells. (iii) UU1250-Tar strain was then used to construct chimera variants with a histamine receptor via Rosetta software computing. A conventional microscopy-based chemotaxis assay was performed on the six highest-scoring variants, represented by each row. The variant that demonstrated the highest chemotactic response to histamine, represented in orange, was chosen for PRISM chemotaxis assays.

encoded synthetic chemoreceptors.[15,16] In this work, we demonstrate a proof-of-concept method to observe real-time, label-free bacterial chemotaxis for the rapid screening of bacteria containing synthetic chemoreceptor variants designed to detect new analytes. Our method utilizes phase-shift reflectometric interference spectroscopic methods, termed PRISM. PRISM employs two-dimensional arrays of silicon lamellar microstructures that are specifically designed to trap bacteria and optically track their presence,[17] providing an abiotic−biotic interface that has been successfully used for monitoring antibiotic susceptibility[18] and protein inclusion body production.[19] In this work, we specifically employ periodic femtoliter well arrays (FMAs) etched in a silicon chip to trap bacterial cells expressing the synthetic chemoreceptors and then expose them to an overhead flow of analyte solution. The FMAs provide an optical transducing element that allows for the refractive index of the media within the wells to be optically monitored by reflected white light,[20] while the overhead analyte solution, termed the chemoeffector, flows. If the chemoeffector serves as a chemoattractant to the seeded bacteria, the cells will swim toward the attractant, leaving the FMAs and resulting in a decrease in refractive index of the FMAs. Conversely, if the chemoeffector serves as a chemorepellent, the cells remain within the protection of the FMAs resulting in an increase in refractive index. These bacterial responses to the change in chemical environment are captured in real-time without the use of fluorescent labels or sophisticated optical detection systems.

Herein, we successfully employ PRISM for the detection of chemotaxis on three synthetic chemotactic *E. coli* variants. First, we characterize the attractant response to L-aspartate of a mutant strain of *E. coli* with all its native chemoreceptors knocked out, and containing a knock-in plasmid expressing the natural Tar chemoreceptor. Second, we demonstrate a repellent response of a native *E. coli* strain to benzoate. Finally, we characterize an attractant response to a synthetic chemoreceptor for histamine encoded on the knock-in plasmid instead of the Tar chemoreceptor.

## RESULTS AND DISCUSSION

**Design and Construction of Chemotactic Variants.** We initially constructed various chemotactic variants, as schematically outlined in Figure 1, in order to test the feasibility of our chemotaxis PRISM assay. Beginning with chemotactically deficient *E. coli* RP437 UU1250 as a parental strain, we designed a UU1250-Tar strain chemotactically responsive to L-aspartate through Gibson Assembly cloning. Successful construction of the plasmid encoding the *tar* chemoreceptor gene was verified by DNA sequencing, while localization of the Tar chemoreceptor[21] to the cell membrane poles was confirmed by the construction of a UU1250-Tar-EGFP (green fluorescence protein) strain, in which an *egfp* gene was fused to the C′ terminus of the *tar* gene using a linker coding for a flexible short peptide (see Methods) to observe where the plasmid-borne chemoreceptor localizes. In Figure 1, we show that Tar-EGFP of step II can be detected in the cell poles, indicating a proper migration and localization of the Tar receptor. In comparison, a typical GFP-expressing *E. coli* strain lacks GFP translocation to the cell poles, while UU1250-Tar did not display any GFP fluorescence (see Figure S1). Next, we confirmed that the UU1250 strain expressing the Tar chemoreceptor is chemotactic using a commercially available chemotaxis assay (see Figure S2). Finally, we confirmed the UU1250 cells remain motile for the long period of time (7 h) in the starvation-motility buffer, which was required for the PRISM assay (see Figure S3).

With the confirmed UU1250-Tar strain, we then constructed a new synthetic chemoreceptor for histamine, a derivative of the amino acid histidine, which is involved in the inflammatory response and is known to be a mediator of itching, by employing the Rosetta macromolecular modeling software suite.[22,23] Rosetta comprises a collection of algorithms and programs for macromolecular modeling and design,


DOI: 10.1021/acsbiomaterials.8b01429
ACS Biomater. Sci. Eng. 2019, 5, 603−612

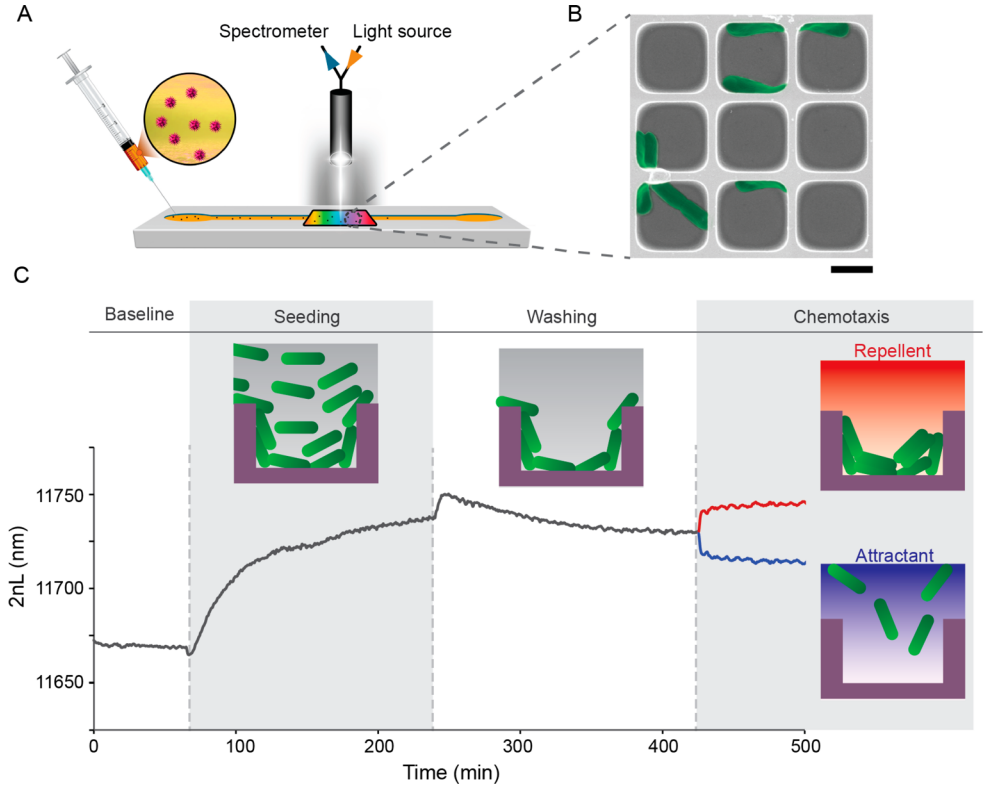


**Figure 2.** Chemotaxis-on-a-chip concept and example results. (A) Photonic chip is housed in a heated flow cell containing an inlet and outlet ports while the zero-order diffractive reflectance of the chip is monitored. (B) Scanning electron microscope image of a photonic chip comprising nine Si femtoliter wells containing *E. coli* cells (cells are false-colored for clarity). Scale bar represents 2 $\mu$m. (C) Characteristic PRISM read-out for a single experiment, presenting all three experimental steps after baseline acquisition: (1) seeding step in which a bacterial suspension is introduced, (2) washing step in which unattached cells are removed using a motility buffer, and (3) chemotaxis step, which includes the addition of a chemoeffector.

allowing us to computationally mutate the L-aspartate binding chemoreceptor (Tar) to design in silico variants that can potentially bind histamine.[24] Briefly, the program is given two inputs, a protein data bank (PDB) file containing the sequence of the ligand-binding domain of the starting chemoreceptor, namely Tar, and the chemical structure of the desired target ligand, which we chose as histamine. The program then inserts random mutations into the sequence of the native binding domain and calculates the effects of these mutations in terms of energy and binding affinity. The output of a single protocol iteration is a library of dozens to hundreds of variants, each with its own set of mutations. We then use a set of filters to select the variants that do not fall in the bottom quartile of any of the filters, and repeat the algorithm until a sufficiently large library of virtual variants is created. For histamine, we ran five iterations of the protocol, to increase the chances of a successful hit, and obtained 450 high-scoring variants. In the final round, we again applied the filtration and the quartile-weaning process and were left with six variants. The six variants were tested using a conventional microscope-based chemotaxis assay, but only the one variant exhibiting a noticeable response to histamine was selected for testing chemotactic responses using the PRISM method. Additional steps of computational designs, calculated mutations, and possibly directed evolution would lead to a more robust, high-affinity chemoreceptor, though for the purpose of studying PRISM as a method of monitoring chemotaxis, the selected variant exhibited a sufficiently high affinity toward histamine. In summary, we redesigned, cloned, and tested a novel UU1250 histamine-Tar chimera chemoreceptor to demonstrate our proof-of-concept chemotaxis PRISM assay.

**Principles of the PRISM Assay for Monitoring Chemotaxis.** The underlying principle of PRISM for monitoring chemotaxis is based on the simultaneous entrance or exit of bacteria from the photonic FMAs toward or away from a chemoeffector and the phase-shift reflectometric interference measurements of the bacteria that remain in the FMAs collected in real time (Figure 2). PRISM assays are performed in a heated microfluidic channel containing a photonic chip fixed in the center (Figure 2A). Each channel contains an inlet port connected to a sample solution reservoir and an outlet port leading to waste and is controlled by a peristaltic pump. The photonic chips are replaced with new clean chips every experiment, with each chip containing arrays of micron-sized wells, which act as a diffraction grating. The FMAs are characterized by square wells ~3.7 $\mu$m in width with an ~0.3 $\mu$m wall, and 4 $\mu$m in depth (volume of ~55 fL), as shown in Figure 2B. For the assays, the chips are illuminated by bifurcated fiber optic, fit with a collimated broadband light source, normally incident to the FMAs. The resulting reflectance spectrum of the illuminated spot (~1.5 mm in diameter) represents the collective optical signal of the bacteria across thousands of wells and is collected by a CCD detector for acquisition by Ocean Optics software. Thus, the location of the light spot on the photonic chip should not cause variance in chemotactic measurements, as the entire chip is continuously and equally subjected to flow of the chemoeffector solution. The reflectance spectrum exhibits an


DOI: 10.1021/acsbiomaterials.8b01429
ACS Biomater. Sci. Eng. 2019, 5, 603−612

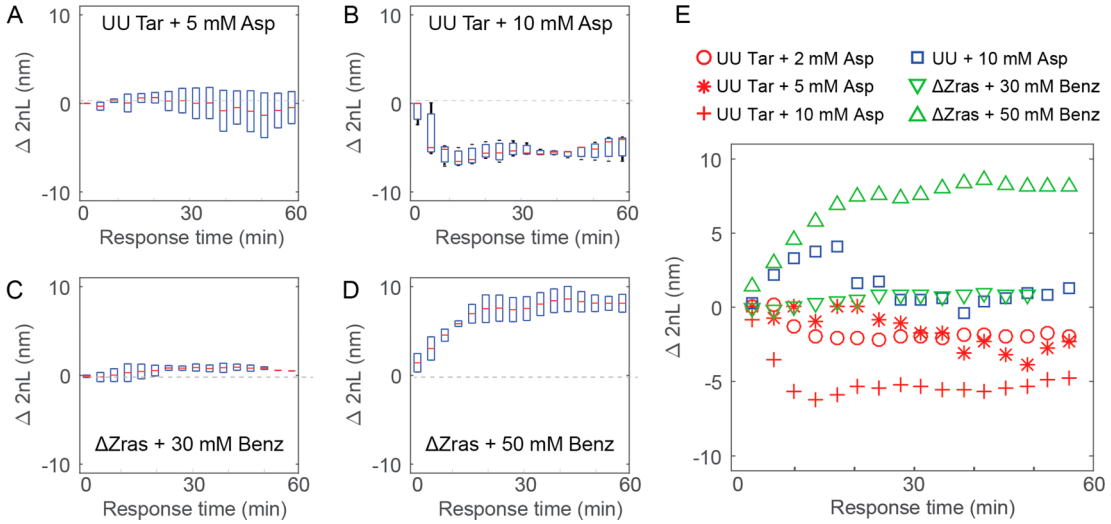


**Figure 3.** Chemotactic responses of *E. coli* strains UU1250-*Tar* and Δ*Zras* to chemoeffectors demonstrated by the PRISM assay expressed as Δ2*nL* over time. (A) Chemotactically responsive UU1250-Tar shows a slight negative Δ2*nL* response to 5 mM L-aspartate, a chemoattractant, after 30 min. (B) A significant negative Δ2*nL* response to 10 mM L-aspartate ensues within 10 min. (C) Contrarily, the chemotactically responsive Δ*Zras* mutant exhibits a slight positive increase in Δ2*nL* in response to the chemorepellent, benzoate, at 30 mM, but a (D) significant, immediate positive response to 50 mM benzoate. (E) Summary of median Δ2*nL* responses for various bacterial strains.

interference pattern characteristic of incident light reflecting partially from the top of the wells and partially reflecting from the bottom of the wells. After applying frequency analysis[17] to the reflected light spectrum, the value 2*nL* is calculated, in which *n* refers to the refractive index of the solution within the wells and *L* represents the depth of the wells. The value of 2*nL* is often regarded as the optical path difference and provides a value for measuring changes in refractive index corresponding to bacterial colonization within the silicon wells. Hence, the presence of bacterial cells within the wells leads to an increase in 2*nL* values, whereas the evacuation of cells out of the wells leads to a decrease in 2*nL*.[17]

The chemotaxis PRISM assays are performed in a three-step process, following the acquisition of a stable baseline measurement in motility buffer (Figure 2C). In the first step (Figure 2C, left panel), termed as the seeding step, a bacterial suspension is introduced into the microfluidic channel and the cells are allowed to settle within the FMAs on the photonic Si chip. This step is characterized by a dramatic increase in the 2*nL* value, which is ascribed to the cells accumulating within the wells. In the subsequent washing step (Figure 2C, middle panel), clean motility buffer is flowed over the chip, leading to a decrease in 2*nL*, as excess, nonadhered cells are removed from the FMAs. In the final step (Figure 2C, right panel), the chemoeffector is introduced. For the case of repellent (Figure 2C, right panel, red trace), when a solution of 50 mM benzoate repellent is introduced, a sharp increase in 2*nL* ensues. This is attributed to loosely attached bacteria cells outside of the sensing region, or more likely, stationary at the top surface, entering the wells. Conversely, in the presence of a chemoattractant, a decrease in 2*nL* is observed (see Figure 2C, right panel, blue trace) as chemotactically responsive cells exit the wells and move into the flow solution. To observe this phenomenon, the cells must be reversibly attached to the surface and/or each other. Although cell attachment to the surfaces agrees with prior observations,[25] in which metabolically tired cells (in this case cells that have been nutrient deprived for 5 h) prefer surface attachment over a planktonic behavior,[26,27] the cells are still able to respond to chemoeffectors and maintain their motility. This suggests that the cells are loosely adhered to the surface.

**PRISM Reveals a Time-Dependent Chemotactic Response to Varying Chemoattractant Concentration.** We studied the chemotactic responses of three *E. coli* strains using PRISM, namely the chemotactically deficient strain UU1250, the engineered UU1250-*Tar* strain, and a chemotactic responsive *E. coli* Δ*zras* strain. The results are depicted in Figure 3, in which Δ2*nL* is calculated as

$$\Delta 2nL = 2nL - 2nL_0 \quad (1)$$

where $2nL_0$ represents the optical path difference at the time in which the chemoeffector is first introduced into the system. In panels A–D, we plot representative time-response functions of 4 different strain/chemoeffector combinations. Each measurement was carried out in triplicates, and the cumulative data is binned into 6 min time intervals plotted as whisker plots of Δ2*nL* response vs time. The red bar in each box corresponds to the median Δ2*nL* response. A varying form of time-response function that depends on strain and concentration of chemoeffector can be observed in the chemotactic responses.

To better understand the dependence of the chemotactic time response on the chemoeffector concentration in PRISM, we plotted the median value of each bin for six strain/chemoeffector combinations in Figure 3E. The *E. coli* strain UU1250-Tar was tested for its chemo-attractive response to 2, 5, and 10 mM of L-aspartate solution. Under the flow of 2 and 5 mM L-aspartate, a slightly decreasing Δ2*nL* response is observed 30 min after introduction of the chemoattractant (red circle and asterisk respectively). However, with 10 mM of L-aspartate (red plus signs), the negative Δ2*nL* response is observed immediately. The negative responses indicate an attractive behavior to L-aspartate, as the seeded cells leave the FMAs and swim toward the flow of the chemoattractant. Contrarily, when the *E. coli* strain Δ*Zras* is exposed to the repellent benzoate at a concentration of 50 mM, a rapid increase in 2*nL* is observed (green triangles). However, no response is observed at a 30 mM benzoate concentration over a 60 min time scale (green upside-down triangles).



DOI: 10.1021/acsbiomaterials.8b01429
ACS Biomater. Sci. Eng. 2019, 5, 603–612

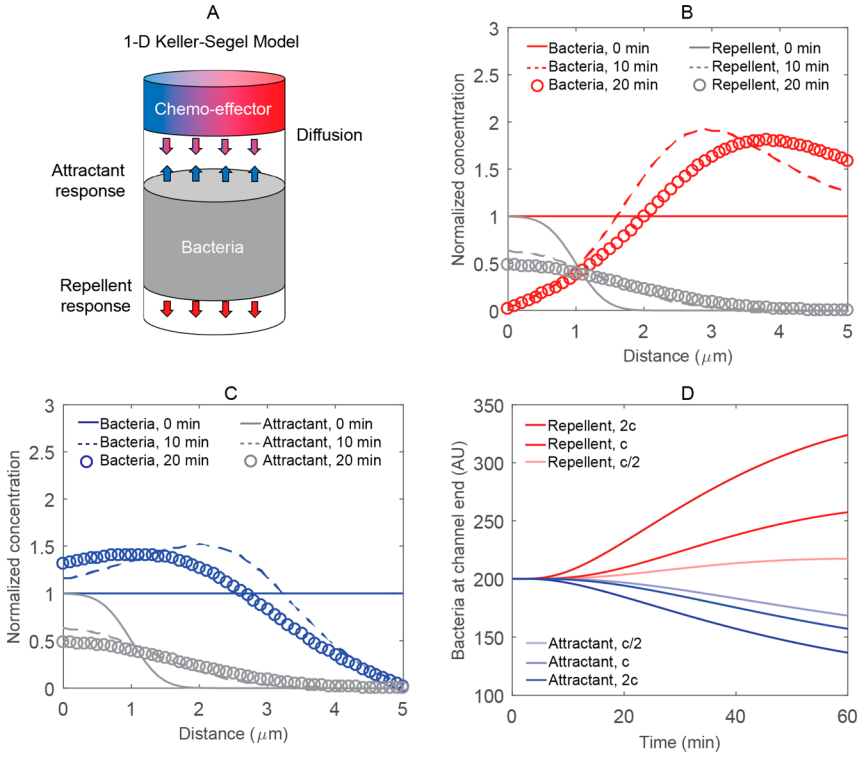


**Figure 4.** One-dimensional Keller−Segel dynamical models for chemotactic responses. (A) Representation of a 1D K−S model in a cylindrical channel. (B) K−S computed responses to a chemorepellent in a 1D semi-infinite channel. After 10 min, a traveling wave of bacteria forms (dotted red line) and after 20 min the wave moves away from the gradient (dashed-dotted red trace). (C) K−S computed responses to a chemoattractant in a 1D semi-infinite channel. After 10 min, a traveling wave of bacteria forms (dotted red trace) and after 20 min the wave moves toward the gradient (dashed-dotted red trace). In both panels, the blue lines (solid, dotted, and dashed-dotted) depict the diffusion of the chemoeffector inside the channel. (D) K−S model predictions for the change of average bacterial concentration inside the pores. We assume that average bacterial concentration is linearly proportional to $\Delta 2nL$. The data depict several predicted time-response curves for simulated chemoattractants and chemorepellents whose concentration range varies over 4×.

Cumulatively, the data reveals that in the PRISM system for both attractants and repellents there exists a threshold concentration, which triggers a rapid response of the cells by either moving into the FMAs to avoid the repellent flow or moving out of the FMAs into the attractant flow. Theoretically, the system is better designed for observing responses to chemoattractants, as more bacteria should be occupied inside the wells as opposed to on the top of the wells, as demonstrated by the increased values of $2nL$ after seeding bacteria and washing nonadhered cells during the stages of the experiment (Figure 2C). This may be one reason as to why the limit of detection for chemotactic responses to an attractant (i.e., UU Tar to L-Aspartate) may be lower than to a repellent (i.e., Δ*zras* to benzoate). In both cases, a stable increase or decrease in $2nL$ values is achieved over time.

**Keller−Segel Simulated Chemotaxis Model.** To understand the dynamics of chemotaxis inside the FMAs, and particularly the dependence of the time-response on a chemoeffector concentration threshold, we simulated the bacterial responses to a gradient of either an attractant or repellent in a cylindrical channel using the dynamical Keller-Segel (K−S) model for chemotaxis[28] (see Methods and schematic illustration in Figure 4A). We approximate the PRISM chemotactic response with a 1D semi-infinite K−S approach where we initially assume the bacteria cells to uniformly occupy the microfluidic channel and that the ligand (analyte) gradient is only applied in one direction. This approximation is adequate for our device, as the average occupancy of the bacteria in the FMAs can be empirically likened to an average change in $2nL$. Thus, when integrated over all the wells, chemotaxis in such a device can emulate a 1D channel. In this continuum approximation of chemotaxis, bacterial motion is modeled via two forms of diffusion: a Brownian and directed diffusion either toward or away from the ligand. As for similar dynamical models, at time zero the attractant or repellent is assumed to be in some initial concentration gradient, and evolution of the bacterial suspension and ligand gradient is subsequently computed.

To investigate if this model can simulate chemotaxis in the photonic FMA chip, we first computed the bacteria and ligand concentration profiles as a function of distance at several time points (see Figure 4B, C) after the introduction of either the repellent or attractant gradient. In Figure 4B we plot the numerical simulation results for the dynamics of the bacterial population (red trace) in the presence of a repellent (gray trace) for three time points. The plot shows that a traveling wave of bacteria forms, moving away from the end where the repellent was at its highest concentration (Figure 4B). This skewed bacterial concentration distribution inside the channel persists and generates a consistently higher concentration of bacteria at the opposite channel end to the one where the repellent was added. Conversely, when the chemotactic response to an attractant is modeled (Figure 4C), a traveling wave of bacteria moving toward the end with the high ligand concentration forms, which in turn leads to a stable depletion


DOI: 10.1021/acsbiomaterials.8b01429
ACS Biomater. Sci. Eng. 2019, 5, 603−612

of the bacterial concentration at the opposite end of the channel for longer time scales.

To further characterize the model's predictions, we reasoned that the $\Delta 2nL$ values are linearly proportional to the average change in bacterial concentration in the FMAs, which is the opposite channel end to the one where the ligand is applied. To obtain a numerical prediction for the $\Delta 2nL$ behavior, we varied the ligand concentration parameter, and computed the predicted bacterial concentration a finite distance from the end of the channel where the attractant or repellent was applied. We plot the results of the predicted bacterial concentration in the channel end in Figure 4D. The figure shows that as the repellent or attractant concentration increases, the bacteria respond more quickly to the gradient in a concentration-dependent fashion, yielding different time-response curves for each chemoeffector type and concentration. In particular, the time-response curve for repellents is characterized by an increasing bacterial concentration inside the wells over time, whereas the one for the attractant is characterized by a decreasing concentration, as a result of the traveling wave of bacteria moving outside of the wells. This prediction indicates that varying concentrations of repellent and attractants can be differentiated by the optical response rate rather than the ultimate level. Experimental observations depicted in Figure 3 affirm this notion, in which bacteria escaping the repellent flow enter the FMAs, thus increasing the measured $2nL$ values; while bacteria swimming toward the attractant leave the FMAs, thus resulting in a decreasing $2nL$ values. Furthermore, due to the concentration-sensitive time-response, the model predicts that the range of concentrations that can be detected will be narrow. Figure 4D shows that for both the simulated repellent and attractant a 4× increase in concentration leads to a substantial deviation in the time-response. This means that characterizing chemotaxis with titrations of several orders of magnitude of ligand concentrations, may not be possible with this dynamical approach. This is consistent with the observation that there seems to be a threshold concentration for both attractants and repellents that triggers a chemotactic response as shown in Figure 3E.

**Confirmation of Designed Histamine-Sensitive Chemoreceptor Using PRISM.** After confirming that PRISM could indeed show chemoattractant and chemorepellent responses, we have constructed six UU1250 His-Tar variants computed by Rosetta, and tested their chemotactic activity toward histamine using PRISM. Out of the six tested variants, one variant mediated an attraction response toward histamine as demonstrated in a box plot representation of two measurements carried out on two biological repeats, where each box is binned over a 6 min window as before (Figure 5A). This response was confirmed for this mutant using a commercial chemotaxis assay and fluorescence pole-migration assays (see Figure S4). Figure 5A reveals a steady decline in the $\Delta 2nL$ response to histamine over time, settling on a value of approximately −5 nm after 60 min. In order to compare this behavior to the native UU1250 Tar-receptor to L-aspartate, we plotted the median $\Delta 2nL$ values, see Figure 5B, for the following PRISM experiments: chemotaxis-deficient UU1250 to 10 mM L-aspartate, UU1250-Tar to 10 mM L-aspartate, and the functional UU1250 His-Tar variant with 5 and 10 mM histamine. The UU1250 His-Tar chimera variant displays a delayed attractant response to L-aspartate, which reaches a steady-state $\Delta 2nL$ level after 45 min, but with a final amplitude that is approximately two times lower than the natural Tar's response to L-aspartate. The UU1250 His-Tar chimera median PRISM response to the addition of histamine results in a moderate and continual change of $\Delta 2nL$, ultimately reaching an amplitude similar to what was observed for the UU1250-Tar's response to aspartate. Consequently, while our new mutant strain displays a clear attractant response to histamine, the original L-aspartate response is not completely abolished. Therefore, at least another round of mutations may be necessary for a uniquely specific histamine strain to be generated (see Figure S5 and the Supporting Information for structural analysis of the Tar-histamine mutant).

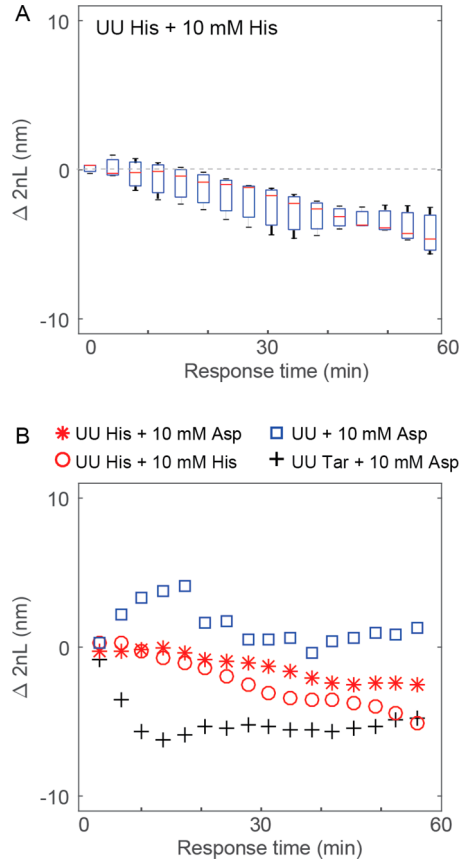


**Figure 5.** Histamine-Tar variant chemotaxis functional analysis via PRISM. (A) Box plot depiction of the UU1250 His-Tar chimera variant (labeled as UU His) in response to 10 mM histamine over time. (B) Median $\Delta 2nL$ values obtained for the chemotactically deficient UU1250 parental strain in response to 10 mM L-aspartate (blue squares), UU1250-Tar strain in response to 10 mM L-aspartate (black plus signs), and the UU1250 His-Tar chimera in response to 10 mM L-aspartate and 10 mM histamine (red stars and red circles, respectively).

## DISCUSSION

We were able to synthesize bacterial mutants and monitor their chemotactic abilities through a new label-free technique, namely PRISM. This method allowed to us to rapidly screen for potential new mutants, which we specifically demonstrated with the histidine binding His-Tar mutant. Though we chose to observe the chemotactic responses of *E. coli*, this assay is not limited by bacterial species and can theoretically be performed to test the responses of any species as long as they are motile and contain chemotaxis receptors (e.g., wild type *Klebsiella* or *Pseudomonas*).


DOI: 10.1021/acsbiomaterials.8b01429
ACS Biomater. Sci. Eng. 2019, 5, 603−612

How does PRISM enable quantitative detection of chemotaxis? In our device the cells are trapped in wells, and as a result one of two scenarios are possible: either the cells reversibly adhere to the surface, or the geometry of the wells prevents them from escaping via diffusion (the cells were shown to be motile even after hours in motility buffer see Figure S3). In both scenarios, the presence of the chemo-attractant plays the role of the "light-at-the-end-of-the-tunnel" which guides the cells motion out of the wells. This interpretation of our results implies that geometry may play a crucial role in the chemotactic response detected with our device. The geometry of the arrangements of the microwells, which also forces us to employ a dynamic and unstable chemical gradient are likely the cause for the two major short-comings of our approach that are currently reported. Namely, the relatively high detection limit (mM concentrations as opposed to nM-$\mu$M), and the apparent imbalance in sensitivity to chemoattractants as oppose to chemorepellents. Therefore, it is possible that modifications to the PRISM chip design, which will allow for a more stable chemical gradient formation can substantially improve the detection threshold for both chemorepellents and chemoattractants. Regardless, we believe that even with the present design, bacterial cultures (e.g., from the gut) can be characterized with the PRISM assay by subjecting them to the mM concentrations as part of diagnostic testing. Though determining the exact concentration of the chemoeffector that affects cells response would be valuable, for many applications, the advantages of having a high-throughput approach outweighs this particular drawback.

Given the rapid recorded responses of the PRISM approach, we envision many potential applications to our work, provided that the preparation time be significantly reduced by optimizing the microfluidics of the flow cell. We believe that complementing our assay with next generation sequencing approaches can provide even more information about the bacterial strain under investigation. Although the relevancy of such hypothetical results to the natural in vivo environment will certainly be questioned, we nevertheless believe that our device can be employed as a new diagnostic and research tool. At the laboratory level, our label-free detection approach can be used to screen for new chemoreceptors as demonstrated here. Furthermore, our system can be readily miniaturized and implemented in a hand-held device for potential rapid and label-free molecular screening (e.g., environmental niches for contaminants and specific molecular cues). By employing a patterned surface that simultaneously captures bacteria and optically monitors the bacteria behavior, we have taken advantage of material−bacterial interactions to guide the synthesis of mutant bacterial cells containing desired chemoreceptors.

## MATERIALS AND METHODS

**Materials and Growth Media.** Motility buffer was composed of 0.1 M $K_2HPO_4$, 0.1 M $KH_2PO_4$, 0.1 mM EDTA, and 0.001 mM methionine in double-distilled water (ddH2O, 18 MΩ). Phosphate buffered saline (PBS) pH 7.2 was prepared by dissolving 17 mM $KH_2PO_4$, 27 mM KCl, 52 mM $Na_2HPO_4$, and 1.4 M NaCl in $ddH_2O$. Super Optimal Broth with Catabolite Repression (SOC) was composed of 2% (w/v) tryptone, 0.5% (w/v) yeast extract, 10 mM NaCl, 2.5 mM KCl, 10 mM $MgCl_2$, and 20 mM glucose. Bioassay buffer (BA) was composed of 0.5 mg/mL tryptone, 0.1 M NaCl, and 1 M MgSO4 in 0.01 M PBS supplemented with 0.03% (w/v) glycerol. Tryptone broth (TB) was composed of 10 g/L tryptone and 10 g/L NaCl. L-aspartate solutions were prepared in motility buffer.

L-aspartate, N′-(3-triimethoxysilylpropyl) diethylenetriamine (DETAS), succinic anhydride, N,N′-diisopropylcarbodiimide (DIC), *N*-hydroxysulfosuccinimide (NHS), lectin from *Triticum vulgaris* (termed as wheat germ agglutinin or WGA), and acetonitrile were purchased from Sigma-Aldrich, Israel. Absolute ethanol, potassium and phosphate salts, dimethyl sulfoxide (DMSO), and diisopropylethylamine (DIEA) were supplied by Merck, Germany. Acetic acid, NaCl, and $MgSO_4$ were supplied by Bio-Lab Ltd., Israel. Bacto agar and tryptone were supplied by BD Biosciences, USA. Low melt SeaPlaque agarose was purchased from Lonza. EDTA was supplied by JT Baker. Sodium benzoate was supplied by Honeywell Fluka.

**Bacterial Strains and Plasmids.** The chemotactically deficient *E. coli* RP437 strain UU1250 [Δ*tsr-7028* Δ*(tar-tap)5201* Δ*trg-100* Δ*aer-1, kan*$^r$][29] was obtained from Dr. Ady Vaknin (Hebrew University, Jerusalem, Israel) and was used as a parental strain to construct UU1250-Tar and UU1250-Tar-EGFP. *E. coli* RP437 strain ΔZras was used to observe chemorepellent behavior and was obtained from Prof. Michael Eisenbach (Weizmann Institute, Rehovot, Israel). Plasmid pSB1C3 was obtained from the iGEM 2016 distribution kit (Biobrick Foundation, Boston, MA). See Table S1 for a comprehensive list of plasmids and strains and construction descriptions.

**Construction of UU1250-Tar Variants.** The Tar expression plasmid was constructed as follows with in-depth details of materials found in Tables S1 and S2. First, a new backbone plasmid pTSB1C3 was constructed using the pSB1C3 backbone and the following parts: *Anderson strong promoter* (BBa_J23100), a strong ribosome binding site (RBS-BBa_K0034) and a double terminator (BBa_B0015). The parts were successively cloned within the original backbone's multiple cloning site using the restriction enzymes *Pst*I, SpeI and XbaI (NEB, USA). Next, the *tar* chemoreceptor gene (BBa_K777000) and the new pTSB1C3 backbone were amplified using the following PCR primers detailed in Figure S5. Finally, a Gibson Assembly reaction was carried out using the Gibson Assembly Master Mix (NEB, USA) to construct the pTSB1C3-*tar* plasmid with the *tar* gene positioned downstream of the Anderson strong promoter, Ribosome Binding Site, and upstream to the double terminator. All plasmids were transformed using heat-shock into *E. coli*-Top 10 (Life Technologies, USA), grown on 25 $\mu$g/mL chloramphenicol (*Cm*) agar plates, and sequence-verified before continuing to the next cloning step. The plasmid pTSB1C3-*tar* was then transformed into the chemotactic deficient UU1250 after sequence verification using heat-shock to obtain the synthetic chemotactic strain as follows: heat-shock competent UU1250 cells were initially incubated on ice for 30 min with 1 nM of the pTSB1C3-*tar* plasmid suspension. Then the cell-plasmid suspension was placed in a 42 °C water bath for 45 s and subsequently placed on ice for an additional 2 min. Next, 900 $\mu$L of SOC was added to the cell-plasmid suspension, transferred to a 15 mL tube, and continued the recovery at 37 °C for 1 h while shaking vigorously. Finally, the cell-plasmid-SOC suspension was plated on 25 $\mu$g/mL *Cm* plates.

The Tar-EGFP chimera was constructed as follows: first, a flexible linker 5′-GGTAGCGGCAGCGGTAGC-3′ sequence was obtained from (Bba J18921) and fused to an EGFP (enhanced green fluorescent protein) gene obtained from (Bba E0040) via a polymerase chain reaction (PCR) using the following primers GFP_OVERHANG_FOR 5′- gaagcggcagcggtagcat gcgtaaaggagaagaac-3′, GFP_OVERHANG_REV 5′- cgttttatttgatgcctggctctagtattatttgtata gttcatccatgc-3′ to make a linker-EGFP fragment. Next, a PCR reaction to the pTSB1C3-Tar plasmid using the detailed primers was performed: TAR_REV_GFP_OP 5′-ctcctttacgcatgctaccgctgccgcttccaaatgtttcccagtttgg −3′ pOpen_P-R-T_for 5′- tactagagccaggcatcaaataaaacg-3′, respectively. Finally, the new pTSB1C3-Tar-EGFP plasmid was constructed using a Gibson Assembly reaction as described above.

**In Silico and Physical Construction of UU1250 Histamine Variants.** To construct the UU1250 Histamine variant in silico, a Rosetta software protocol by Moretti et al.[30] was followed using the Worldwide LHC computing grid. The output of the protocol consists of a library of variants, ranging from dozens to thousands of protein data bank files, depending on the parameters of the design. Selection


DOI: 10.1021/acsbiomaterials.8b01429
ACS Biomater. Sci. Eng. 2019, 5, 603−612

of in silico variants proceeded as a virtually directed evolution experiment with successive rounds of virtual evolution of the parent variants starting with the original Tar protein. The protocol was designed as follows: First, starting from the Tar sequence, Rosetta computed the top 100 variants that scored as potential binders to histamine. We then selected a set of 16 parameters (see Table S3) computed by Rosetta for further filtration of the results. We kept only the variants that were scored in top 3 quartiles (75%) for any of the 16 parameters. This selection process resulted in three variants that were used as virtual parents for the next computation cycle. We repeated this process of computation, filtration, and selection for a total of 5 cycles until a library of ∼500 high-scoring, virtual-histamine-binding variants was generated. We then used the quartile filtration step to select 6 histamine-binding variants to use for real DNA synthesis, cloning, and chemotaxis analysis.

The six putative mutants of the histamine-binding Tar variant were then physically constructed by mutating the native Tar chemoreceptor at amino acid positions 25−40 and 95−123 in two stages. The mutation process was performed using two sets of forward and reverse overlapping primers in two sets of PCR reactions as shown in Table S2. First, a mutation of Tar chemoreceptor pTSB1C3-*tar* at amino acid positions 25−40 was performed via a single PCR reaction using a set of primers containing the six different sets of mutations (described in Table S3). Then, the mutated pTSB1C3-*tar* plasmid was ligated to reform a closed plasmid and transformed into heat-shocked *E. coli*-Top 10. After sequence verification of the transformed *E. coli* -Top 10, the second mutation of the Tar chemoreceptor pTSB1C3- *tar* at amino acid positions 95−123 was carried out on the subset of mutated Tar clones using another set of primers containing the relevant mutations. Lastly, variants containing both mutated regions were transformed into the UU1250 strain using the methods described above for pTSB1C3- *tar*.

**Fabrication of Photonic Well Arrays.** Photonic silicon chips containing arrays of square femtoliter wells were fabricated by standard lithography and reactive ion etching techniques at the Micro-Nano- Fabrication and Printing Unit, Technion − Israel Institute of Technology and mechanically diced into 10 mm by 5 mm chips by an automated dicing saw (Disco, Japan). Lectin from *tritium vulgaris*, commonly referred to as wheat germ agglutinin (WGA), was immobilized on the Si surface as previously described.[31] Briefly, the chips were thermally oxidized in ambient air at 800 °C for 1 h in a Lindberg/Blue Split-Hinge furnace (Thermo Scientific, USA), followed by silanization in 2% N′-(3-triimethoxysilylpropyl) diethylenetriamine (50% ethanol in dd$H_2O$, acidified with 0.6% acetic acid) for 1 h. Chips were washed with ethanol and dried under a stream of nitrogen. Carboxylation was performed by incubation in a solution comprised of 1% succinic anhydride (in acetonitrile with 4% DIEA) for 3 h followed by washing with ethanol and drying with nitrogen. Amine activation was promoted by incubation in 129 mM N,N′-diisopropylcarbodiimide and 87 mM *N*-hydroxysulfosuccinimide constituted in acetonitrile for 1 h. After rinsing with ethanol, chips were stored at 4 °C overnight in WGA solution (1 mg/mL, 10% DMSO) to promote lectin immobilization onto the Si wells.

**Chemotactic Responses Captured by Real-Time PRISM.** Because of the micrometer-sized dimensions of the femtoliter wells, the arrays act as a two-dimensional Si diffraction grating that can be employed for intrinsic, real-time optical measurements. Thus, we employed phase-shift reflectometric interference spectroscopic measurements, referred to as PRISM,[18] to accurately measure chemotactic responses in real-time. To do so, a photonic silicon chip containing the FMAs was fixed in a custom-made flow cell heated to 37 °C and illuminated by a broadband tungsten light source (OceanOptics, LS-1) normal to the surface. Zero-order diffraction was measured as a function of reflectance intensity versus wavelength and was collected by a CCD spectrometer (OceanOptics, USB4000). Using frequency analysis[17] the value $2nL$ was calculated, in which $n$ refers to the refractive index of the solution within the wells and $L$ represents the depth of the wells. The value of $2nL$ is often regarded as the optical path difference and provides a value for measuring changes in refractive index corresponding to bacterial colonization within the silicon wells. Hence, upon the presence of bacterial cells within the wells leads to an increase in $2nL$ values, whereas the evacuation of cells out of the wells leads to a decrease in $2nL$.[17]

All solutions were delivered to the photonic chips at a flow rate of ∼0.3 mL/min pulled by a peristaltic pump. After acquisition of stable baseline $2nL$ values in clean motility buffer for 45 min through the flow cell, chemotaxis assays were performed in the following three stages while reflectance spectra were recorded (as outlined in Figure 1): First, during the cell seeding stage, a bacterial suspension prepared in motility buffer ($OD_{600}$ ∼ 1) was continuously delivered to the photonic chip until the wells were saturated with bacterial cells as indicated by the $2nL$ values; Second, during the washing stage, the chip was washed by flowing only motility buffer to remove loosely adhered cells or nonattached cells; Lastly, during the chemotaxis stage, the chemoeffector solution made in motility buffer, was delivered to the chip for approximately 30 min through the input inlet. Chemotactic responses were measured as a function of $\Delta 2nL$ with

$$\Delta 2nL = 2nL - 2nL_0 \tag{1}$$

where $2nL_0$ is the optical path difference measured at $t = 0$, which was assigned to the time in which the chemoeffector solution was first introduced into the flow cell.

**Computational Simulation of Chemotaxis in Femtoliter Microwells.** We employed the classical Keller-Segel (KS) chemotaxis model for a 1D semi-infinite channel[32] to model chemotactic responses in the femtoliter wells. The KS model is described by the following coupled partial differential equations:

$$\frac{\partial U}{\partial t} = \nabla(k_1 \nabla U - k_2 U \nabla V) + k_3 \tag{2}$$

$$\frac{\partial V}{\partial t} - D\frac{\partial^2 V}{\partial X^2} = \delta(x)\delta(t)\int_0^\infty V(x', t)\mathrm{d}x' \tag{3}$$

in which $U$ is bacteria concentration, $V$ is the chemoeffector concentration, $k_1$ is the bacterial Brownian diffusion coefficient, $k_2$ is the chemotactic response coefficient, $k_3$ is bacterial population coefficient (i.e., division and cell death), and $D$ is the chemoeffector diffusion coefficient. For modeling, we used $D = 1 \times 10^{-9}$ $m^2/s$, which is the estimated diffusion rate for small molecules in water, $k_1 = 2 \times 10^{-9}$ $m^2/s$, and $k_2 = \pm 10^{-8}$ $m^5/s$ for the chemoattractant (+) and chemorepellent (−) respectively.[33] The model operates under the following assumptions: $k_2$ controls the sensitivity of the response to changes in chemorepellent/chemoattractant concentration; the femtoliter wells have a cylindrical symmetry allowing the problem to be solved in 1D; bacterial life and death are neglected ($k_3 = 0$) for the duration of the simulated run ($t < 60$ min). The average bacteria life/death time scales are ∼5× longer in motility buffer than the 60 min run time of the model; chemorepellent/chemoattractant concentration is controlled only by diffusion; the bacteria do not consume the chemorepellent/chemoattractant; there are no changes in bacterial concentration at the edges of the channel; and bacteria are uniformly distributed in the channel at the time $t = 0$. The initial chemoeffector concentration and bacteria concentration are designated as 0. The boundary conditions used are as follows for all $t > 0$:

$$\frac{\partial U}{\partial x}(0, t) = 0 \tag{4}$$

$$\frac{\partial U}{\partial x}(x_{end}, t) = 0 \tag{5}$$

Under the specified assumptions and using the parameters as described above, the solution to the chemorepellent/chemoattractant concentration is given by a combination of error functions:

$$V(x, t) = \frac{V_0}{2}\left[\mathrm{erf}\left(\frac{x + 2h}{\sqrt{4Dt}}\right) - \mathrm{erf}\left(\frac{x}{\sqrt{4Dt}}\right)\right] \tag{6}$$

in which $V_0$ is the initial chemorepellent/chemoattractant concentration, normalized to 1. The parameter $h$ is defined as the ratio



DOI: 10.1021/acsbiomaterials.8b01429
ACS Biomater. Sci. Eng. 2019, 5, 603−612

between the sample volume and the channel cut section and was assigned to $h = 1 \times 10^{-6}$ m meaning that the channel opening is filled to capacity. Given eq 6, the chemoeffector concentration is known for any time and position. Plugging this information into the Keller-Segel model (eq 3) results in a partial differential equation dependent only on $U(x,t)$. This equation was solved discretely using Matlab (code available upon request).

**Conventional Microscopic Analysis of Chemotaxis Using Ibidi Slides.** Bacterial strains were grown overnight at 30 °C in TB supplemented with the appropriate antibiotic, then diluted in a 1:50 ratio, and regrown to an $OD_{600} \sim 1$. A 160 μL suspension of bacteria made in motility buffer was injected into a commercial sticky-Slide I Luer (Ibidi, Germany) designed for perfusion applications. The Sticky-Slides were prepared according to the manufacture's specifications. After which, 40 μL of a chemoeffector was pipetted into the microfluidic channel. Images of bacterial responses to chemoeffectors at the point 3 mm from the outlet of the channel were acquired every 30 s for 20 min using a Nikon Eclipse Ti microscope at 100× magnification in DIC mode.

**Imaging.** EGFP was imaged using an excitation wavelength of 490 nm and emission of 510 nm. HR-SEM was performed after fixation of a photonic chip with 2.5% glutaraldehyde in PBS, followed by washing with water and a series of ethanol dilutions (50−70−100%) for 2 min. The dried sample was observed by an Ultra Plus high-resolution scanning electron microscope equipped with a Schottky field-emission gun (Carl Zeiss, Germany) operating at an acceleration voltage of 1 kV.

## ■ ASSOCIATED CONTENT

### Supporting Information

The Supporting Information is available free of charge on the ACS Publications website at DOI: 10.1021/acsbiomaterials.8b01429.

Description of commercial chemotaxis assays that corroborates the finding with PRISM; commercial chemotaxis assay applied to both the Tar and Tar-histamine variants; structural analysis of the mutations in the Tar chemoreceptor leading to histamine binding; Figures S1−S5; Tables S1−S3 (PDF)

## ■ AUTHOR INFORMATION


### Corresponding Authors

*Email: roeeamit@bfe.technion.ac.il.

*E-mail: tzila937@campus.technion.ac.il.

### ORCID

Heidi Leonard: 0000-0003-2461-6822

Ester Segal: 0000-0001-9472-754X

Roee Amit: 0000-0003-0580-7076


### Author Contributions

†T.D., N.G., S.Z., and H.L. contributed equally. The manuscript was written through contributions of all authors. All authors have given approval to the final version of the manuscript.

### Notes

The authors declare no competing financial interest.

## ■ ACKNOWLEDGMENTS

We thank the Department of Biotechnology and Food Engineering at the Technion−Israel Institute of Technology for allocating laboratory space. We gratefully acknowledge the financial support of the Lorry I. Lokey Interdisciplinary Center for Life Sciences and Engineering, Technion president Prof. Peretz Lavie, and the Israeli Ministry of Science, Technology and Space for funding. We also thank Dr. Nadav Ben Dov and Dr. Naama Massad-Ivanir from the Department of Biotechnology and Food Engineering for their guidance and Orna Ternyak and Dima Peselev of the Micro- Nano- Fabrication and Printing Unit at the Technion−Israel Institute of Technology for the fabrication of the photonic chips.

## ■ REFERENCES


(1) Hazelbauer, G. L.; Falke, J. J.; Parkinson, J. S. Bacterial chemoreceptors: high-performance signaling in networked arrays. *Trends Biochem. Sci.* **2008**, *33* (1), 9−19.

(2) Alon, U.; Surette, M. G.; Barkai, N.; Leibler, S. Robustness in bacterial chemotaxis. *Nature* **1999**, *397* (6715), 168−71.

(3) Kohler, S.; Belkin, S.; Schmid, R. D. Reporter gene bioassays in environmental analysis. *Fresenius' J. Anal. Chem.* **2000**, *366* (6−7), 769−779.

(4) Turner, K.; Xu, S. F.; Pasini, P.; Deo, S.; Bachas, L.; Daunert, S. Hydroxylated polychlorinated biphenyl detection based on a genetically engineered bioluminescent whole-cell sensing system. *Anal. Chem.* **2007**, *79* (15), 5740−5745.

(5) Courbet, A.; Endy, D.; Renard, E.; Molina, F.; Bonnet, J. Detection of pathological biomarkers in human clinical samples via amplifying genetic switches and logic gates. *Sci. Transl. Med.* **2015**, *7* (289), No. 289ra83.

(6) Drachuk, I.; Suntivich, R.; Calabrese, R.; Harbaugh, S.; Kelley-Loughnane, N.; Kaplan, D. L.; Stone, M.; Tsukruk, V. V. Printed Dual Cell Arrays for Multiplexed Sensing. *ACS Biomater. Sci. Eng.* **2015**, *1* (5), 287−294.

(7) Sourjik, V.; Berg, H. C. Binding of the Escherichia coli response regulator CheY to its target measured in vivo by fluorescence resonance energy transfer. *Proc. Natl. Acad. Sci. U. S. A.* **2002**, *99* (20), 12669−12674.

(8) Mao, H.; Cremer, P. S.; Manson, M. D. A sensitive, versatile microfluidic assay for bacterial chemotaxis. *Proc. Natl. Acad. Sci. U. S. A.* **2003**, *100* (9), 5449−5454.

(9) Seymour, J. R.; Ahmed, T.; Marcos; Stocker, R. A microfluidic chemotaxis assay to study microbial behavior in diffusing nutrient patches. *Limnol. Oceanogr.: Methods* **2008**, *6* (9), 477−488.

(10) Kim, M.; Kim, T. Diffusion-Based and Long-Range Concentration Gradients of Multiple Chemicals for Bacterial Chemotaxis Assays. *Anal. Chem.* **2010**, *82* (22), 9401−9409.

(11) Englert, D. L.; Manson, M. D.; Jayaraman, A. Flow-Based Microfluidic Device for Quantifying Bacterial Chemotaxis in Stable, Competing Gradients. *Appl. Environ. Microbiol.* **2009**, *75* (13), 4557−4564.

(12) Diao, J.; Young, L.; Kim, S.; Fogarty, E. A.; Heilman, S. M.; Zhou, P.; Shuler, M. L.; Wu, M.; DeLisa, M. P. A three-channel microfluidic device for generating static linear gradients and its application to the quantitative analysis of bacterial chemotaxis. *Lab Chip* **2006**, *6* (3), 381−388.

(13) Roggo, C.; Picioreanu, C.; Richard, X.; Mazza, C.; van Lintel, H.; van der Meer, J. R. Quantitative chemical biosensing by bacterial chemotaxis in microfluidic chips. *Environ. Microbiol* **2018**, *20*, 241−258.

(14) Li, J.; Go, A. C.; Ward, M. J.; Ottemann, K. M. The chemical-in-plug bacterial chemotaxis assay is prone to false positive responses. *BMC Res. Notes* **2010**, *3* (1), 77.

(15) Bi, S.; Pollard, A. M.; Yang, Y.; Jin, F.; Sourjik, V. Engineering Hybrid Chemotaxis Receptors in Bacteria. *ACS Synth. Biol.* **2016**, *5* (9), 989−1001.

(16) Bi, S.; Yu, D.; Si, G.; Luo, C.; Li, T.; Ouyang, Q.; Jakovljevic, V.; Sourjik, V.; Tu, Y.; Lai, L. Discovery of novel chemoeffectors and rational design of Escherichia coli chemoreceptor specificity. *Proc. Natl. Acad. Sci. U. S. A.* **2013**, *110* (42), 16814−9.

(17) Massad-Ivanir, N.; Mirsky, Y.; Nahor, A.; Edrei, E.; Bonanno-Young, L. M.; Ben Dov, N.; Sa'ar, A.; Segal, E. Trap and track: designing self-reporting porous Si photonic crystals for rapid bacteria detection. *Analyst* **2014**, *139* (16), 3885−3894.




DOI: 10.1021/acsbiomaterials.8b01429
*ACS Biomater. Sci. Eng.* 2019, 5, 603−612

(18) Leonard, H.; Halachmi, S.; Ben-Dov, N.; Nativ, O.; Segal, E. Unraveling Antimicrobial Susceptibility of Bacterial Networks on Micropillar Architectures Using Intrinsic Phase-Shift Spectroscopy. *ACS Nano* **2017**, *11* (6), 6167−6177.
(19) Ude, C.; Ben-Dov, N.; Jochums, A.; Li, Z.; Segal, E.; Scheper, T.; Beutel, S. Online analysis of protein inclusion bodies produced in E. coli by monitoring alterations in scattered and reflected light. *Appl. Microbiol. Biotechnol.* **2016**, *100* (9), 4147−4159.
(20) Mirsky, Y.; Nahor, A.; Edrei, E.; Massad-Ivanir, N.; Bonanno, L. M.; Segal, E.; Sa'ar, A. Optical biosensing of bacteria and cells using porous silicon based, photonic lamellar gratings. *Appl. Phys. Lett.* **2013**, *103* (3), 033702.
(21) Shiomi, D.; Yoshimoto, M.; Homma, M.; Kawagishi, I. Helical distribution of the bacterial chemoreceptor via colocalization with the Sec protein translocation machinery. *Mol. Microbiol.* **2006**, *60* (4), 894−906.
(22) Schueler-Furman, O.; Wang, C.; Bradley, P.; Misura, K.; Baker, D. Progress in Modeling of Protein Structures and Interactions. *Science* **2005**, *310* (5748), 638−642.
(23) Leaver-Fay, A.; Tyka, M.; Lewis, S. M.; Lange, O. F.; Thompson, J.; Jacak, R.; Kaufman, K. W.; Renfrew, P. D.; Smith, C. A.; Sheffler, W.; Davis, I. W.; Cooper, S.; Treuille, A.; Mandell, D. J.; Richter, F.; Ban, Y.-E. A.; Fleishman, S. J.; Corn, J. E.; Kim, D. E.; Lyskov, S.; Berrondo, M.; Mentzer, S.; Popović, Z.; Havranek, J. J.; Karanicolas, J.; Das, R.; Meiler, J.; Kortemme, T.; Gray, J. J.; Kuhlman, B.; Baker, D.; Bradley, P., Chapter nineteen - Rosetta3: An Object-Oriented Software Suite for the Simulation and Design of Macromolecules. In *Methods in Enzymology*; Johnson, M. L., Brand, L., Eds.; Academic Press: 2011; Vol. *487*, pp 545−574.
(24) Moretti, R.; Bender, B. J.; Allison, B.; Meiler, J., Rosetta and the Design of Ligand Binding Sites. In *Computational Design of Ligand Binding Proteins*; Stoddard, B. L., Ed.; Springer: New York, 2016; pp 47−62.
(25) Lotan, R.; Sharon, N.; Mirelman, D. Interaction of Wheat-Germ Agglutinin with Bacterial Cells and Cell-Wall Polymers. *Eur. J. Biochem.* **1975**, *55* (1), 257−262.
(26) Petrova, O. E.; Sauer, K. Sticky Situations: Key Components That Control Bacterial Surface Attachment. *J. Bacteriol.* **2012**, *194* (10), 2413−2425.
(27) Hall-Stoodley, L.; Costerton, J. W.; Stoodley, P. Bacterial biofilms: From the natural environment to infectious diseases. *Nat. Rev. Microbiol.* **2004**, *2* (2), 95−108.
(28) Keller, E. F.; Segel, L. A. Model for Chemotaxis. *J. Theor. Biol.* **1971**, *30* (2), 225−234.
(29) Ames, P.; Studdert, C. A.; Reiser, R. H.; Parkinson, J. S. Collaborative signaling by mixed chemoreceptor teams in Escherichia coli. *Proc. Natl. Acad. Sci. U. S. A.* **2002**, *99* (10), 7060−7065.
(30) Moretti, R.; Bender, B. J.; Allison, B.; Meiler, J. Rosetta and the Design of Ligand Binding Sites. *Methods Mol. Biol.* **2016**, *1414*, 47−62.
(31) Ude, C.; Ben-Dov, N.; Jochums, A.; Li, Z. P.; Segal, E.; Scheper, T.; Beutel, S. Online analysis of protein inclusion bodies produced in E-coli by monitoring alterations in scattered and reflected light. *Appl. Microbiol. Biotechnol.* **2016**, *100* (9), 4147−4159.
(32) Keller, E. F.; Segel, L. A. Model for chemotaxis. *J. Theor. Biol.* **1971**, *30* (2), 225−34.
(33) Berg, H. C. *E. coli in Motion*; Springer: New York, 2004.



DOI: 10.1021/acsbiomaterials.8b01429
*ACS Biomater. Sci. Eng.* 2019, 5, 603−612